Article

Numerical simulation of the fracture behaviour of high-performance fibre reinforced concrete by using a cohesive-crack-based inverse analysis.

Alejandro Enfedaque[1*], Marcos G. Alberti[2], Jaime C. Gálvez[3] and Pedro Cabanas[4,]

[1] Departamento de Ingeniería Civil: Construcción, E.T.S de Ingenieros de Caminos, Canales y Puertos, Universidad Politécnica de Madrid. c/ Profesor Aranguren, s/n, 28040, Madrid, España, Alejandro.enfedaque@upm.es
[2] Departamento de Ingeniería Civil: Construcción, E.T.S de Ingenieros de Caminos, Canales y Puertos, Universidad Politécnica de Madrid. c/ Profesor Aranguren, s/n, 28040, Madrid, España, marcos.garcia@upm.es.
[3] Departamento de Ingeniería Civil: Construcción, E.T.S de Ingenieros de Caminos, Canales y Puertos, Universidad Politécnica de Madrid. c/ Profesor Aranguren, s/n, 28040, Madrid, España, jaime.galvez@upm.es
[4] Cranfield University, College Road, Cranfield, Great Britain B MK43 0AL. pedro.cabanas.116@cranfield.ac.uk

* Correspondence: alejandro.enfedaque@upm.es; +34 910 674 007

Abstract: Fibre reinforced concrete (FRC) has become an alternative for structural applications due its outstanding mechanical properties. The appearance of new types of fibres and the fibre cocktails that can be configured mixing them has created FRC that clearly exceed the minimum mechanical properties required in the standards. Consequently, in order to take full advantage of the contribution of the fibres in construction projects, it is of great interest to have constitutive models that simulate the behaviour of the materials. This study aimed to simulate the fracture behaviour of five types of FRC, three with steel hooked fibres, one with a combination of two types of steel fibres and one with a combination of polyolefin fibres and two types of steel fibres, by means of an inverse analysis based on the cohesive crack approach. The results of the numerical simulations defined the softening functions of each FRC formulation and have pointed out the synergies that are created through use of fibre cocktails. The information obtained might suppose a remarkable advance for designers using high-performance FRC in structural elements.

Keywords: fibre reinforced concrete, simulation, cohesive crack, fibre cocktail.

1. Introduction

Fibre reinforced concrete (FRC) can be considered a composite material as it merges two materials seeking to improve the properties that they individually have. While the plain concrete matrix provides the stiffness and the compressive strength, the fibres enhance the reduced tensile strength and brittleness of plain concrete. The result of this combination is a material with a remarkable compressive strength, and an improved flexural and tensile strength, ductility, toughness and impact resistance among other characteristics. [1-3]. Several studies have pointed out that the improvement of properties that the fibres provide to FRC depend on several factors such as their modulus of elasticity, constituent material, strength, fibre geometry, orientation, dosage, etcetera [4-6].

Among all the available types of fibres suitable for being added to concrete, steel fibres, when added to concrete forming steel fibre reinforced concrete (SFRC), have been the most used ones in structural applications such as footbridges, pavements or tunnel linings [7-9]. In these applications steel fibres prevent crack propagation and brittle failure providing concrete with a determined strength and ductility after cracking. Moreover, polymer fibres such as PVA or polyolefin ones have proved to be a suitable alternative for

 doi:10.20944/preprints202111.0566.v1

structural uses and also might have less durability issues in chemically hazardous environments such as marine ones [10-12]. Another possibility that has been recently explored is using combinations of fibres, the so-called fibre cocktails, in order to obtain high performance FRC with tailor made properties. Several authors have studied the mechanical properties of fibre cocktails of micro and macro steel fibres with outstanding results [13-15]. Fibre cocktails composed by polymer and steel fibres have been also studied being already available papers dealing with concrete formulations that combined polypropylene and steel fibres. In most cases, such mixture aimed at complementing the structural characteristics of steel fibres with a reduced drying and plastic shrinkage or an improved fire resistance [16, 17].

As it has been mentioned in the previous paragraph, outstanding FRC properties might be obtained by mixing different types of fibres but in all cases, if a structural application is sought, the material properties must comply with certain requirements set in standards. There are national standards and structural design recommendations that establish the minimum mechanical properties that a certain type of FRC should meet to take advantage of the contribution of the fibres to the material properties [18-20]. However, in order to fully exploit the mechanical properties that the fibre cocktails provide it is also necessary to provide reliable constitutive models that can be used in the structural design. According to some authors it would be advisable to implement such constitutive models in computer programmes for performing non-linear analysis. In such study, the authors used an analytical inverse analysis, based on the cohesive crack approach, which identified the mechanical and fracture properties required for performing an advanced analysis [21]. In other studies, this matter was approached performing an analytical inverse analysis [22].

Following that rationale this paper seeks to numerically replicate the three-point bending fracture behaviour of the same plain concrete with 0.89% volume fraction of OL, 3D and 5D steel fibres respectively. To achieve this goal experimental data found in literature were employed. In order to simulate the material behaviour, the suitability of using multilinear softening functions to represent the σ-w relation of the mentioned types of SFRC had to be determined. Moreover, once the previous tasks were fulfilled the constitutive model of the same plain concrete with a binary and ternary cocktail of fibres was found. Moreover, a discussion regarding the differences among the softening functions and their relationship with the fibre geometry was carried out.

The significance of this research relies in the potential optimisation of the structural design that might be achieved by implementing the constitutive models in structural design software. A more intense use of the material properties might result in remarkable reductions, or even to total substitution, of the steel-bar reinforcement without compromising the reliability in FRC structural elements. The reduction of the amount of steel used might suppose not only a decrease in the economic costs but also in an increment of the sustainability of the structure due to the savings in raw materials, safety and improvements of durability.

2. Material production and experimental campaign

This section will briefly present the manufacturing process of the concrete formulations which fracture behaviour was simulated in the following sections. A detailed description of the materials used and the steps taken can be seen in [23].

Five formulations of self-compacting FRC were prepared adding several fibre combinations to the same plain concrete formulation. Such plain concrete was designed considering three aggregate types: two types of gravel with particle sizes between 4-8 mm and 4-12 mm respectively and one type of sand with particle sizes between 0-2 mm. The maximum size of the aggregates was 12.7mm. In addition, limestone powder was employed seeking to enhance the workability of the mixes. In all formulations a Portland cement type EN 197-1 CEM I 52.5 was used as binder. A policarboxylic superplasticiser was added to the formulations pursuing to achieve the self-compactability of all types of

Preprints (www.preprints.org) | NOT PEER-REVIEWED | Posted: 30 November 2021 doi:10.20944/preprints202111.0566.v1

concrete while in fresh state. Tap water was also employed in concrete production. The proportions of all components can be seen in Table 1.

Table 1. Plain concrete formulation

Component	Weight (kg/m³)
Water	199
Cement	425
Limestone filler	210
Sand	947
Gravel	292
Finer gravel	194
Superplasticizer	5.91

Three types of fibres (OL, 3D and 5D) were used in order to obtain three types of SFRC. Such formulations were termed SFRC-OL, SFRC-3D and SFRC-5D respectively. In addition, two fibre cocktails were employed in the other two formulations. One of the hybrid formulations, which was named H1, was obtained by mixing OL and 5D fibres. The other hybrid formulation employed OL, 5D and polyolefin fibres (PF). This last formulation was called H2. The fibres characteristics and their appearance can be seen in Table 2 and Figure 1 respectively.

Table 2. Fibre characteristics

	OL	3D	5D	PF
Material	Steel	Steel	Steel	Polyolefin
Shape	Straight	Hooked	Double-hooked	Straight
Length (mm)	13	30	60	60
Eq. diameter (mm)	0.2	0.38	0.9	0.9
Tensile strength (MPa)	>2600	>1160	>2300	>500
Modulus of elasticity (GPa)	210	210	210	9
Fibres per kg.	282,556	3183	3132	27,000

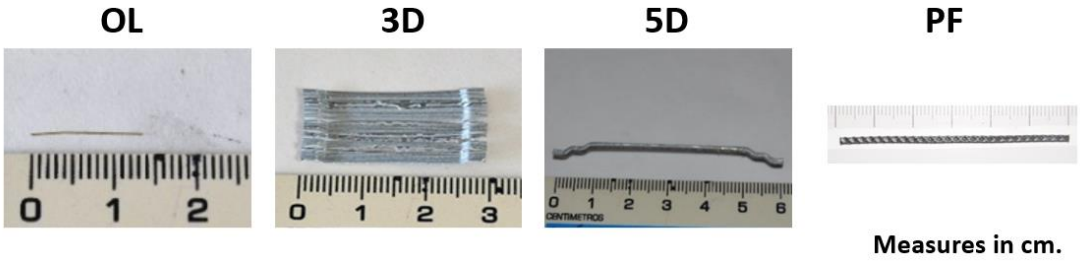

Figure 1. Appearance of the fibres used.

The five concrete formulations were designed seeking to obtain high-performance concrete that were capable of surpassing the requirements set in the most common standards [18-20] for reducing or even eliminating the steel reinforcing bars. Consequently, the volume fraction of fibres added was equal to 0.89% in all concrete types. It should be pointed out that all the formulations were designed to meet the requirements that are set for self-compacting concrete while in fresh state. As it was previously stated, three concrete types were SFRC with only one type of fibre and the other two were concrete types where a cocktail of fibres had been added. In H1 formulation the volume fraction of OL and 5D fibres were equal to 0.445% and their sum was equal to 0.89%. Similarly, H2 had equal volume fractions of OL, 5D and PF, being each one 0.293%, which is a volume fraction of 0.89% combined. It can be observed that the experimental campaign had as main target to characterise the mechanical behaviour of high-performance FRC and also analyse the synergies and improvements that could be obtained by combining several fibre types.

All concrete batches were manufactured in a planetary mixer following the same scheme. A thorough description of the process can be seen in [23]. From each batch six cylindrical specimens of 150 mm of diameter and 300 mm of height were cast. In addition,

Preprints (www.preprints.org) | NOT PEER-REVIEWED | Posted: 30 November 2021 doi:10.20944/preprints202111.0566.v1

four prismatic specimens of dimensions and 600 x 150 x 150 mm³ were also manufactured. All specimens were cured in a climatic chamber until 28 days of age. The cylindrical specimens were used to obtain the compressive strength, the modulus of elasticity and the tensile strength following EN 12390-3 [24], EN 12390-13 [25] and EN 12390-6 [26] respectively. All tests were conducted at 28 days of age of the material. In Table 3 the results of the mentioned tests can be seen.

Table 3. Mechanical properties of the concrete types.

Formulation	f_{cm}		E		f_{ct}	
	(MPa)	c.v.	(GPa)	c.v.	(MPa)	c.v.
SFRC-OL	66.9	0.05	32.8	0.01	7.15	0.03
SFRC-3D	63.1	0.04	32.7	0.02	7.96	0.04
SFRC-5D	63.8	0.02	33.9	0.02	7.69	0.09
H1	64.7	0.02	40.7	0.03	8.05	0.01
H2	66.3	0.03	29.5	0.01	7.95	0.01

As can be seen in Table 3 there were no remarkable differences in the compressive strength of all the formulations tested. Likewise, no notable changes of the tensile strength were found among the mixes. On the contrary, regarding the modulus of elasticity it should be highlighted that H1 boasted a modulus of elasticity that was clearly superior to the ones found in the other concrete types. However, for the purpose of this manuscript, such changes are of minor influence as the modulus of elasticity only possess a remarkable influence in the initial part of the fracture behaviour under a three-point bending setup.

The fracture behaviour was determined following the process shown in [27]. The results of the tests boasted a limited scattering, and the average of the results can be seen in Figure 2.

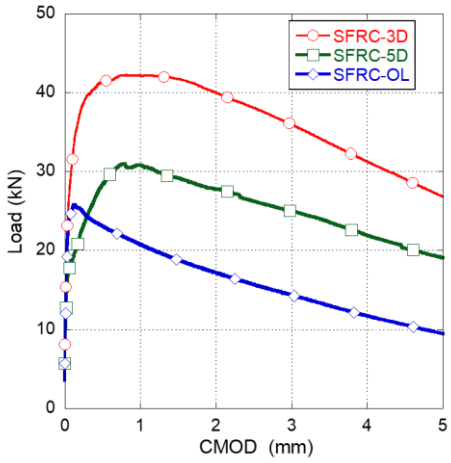

Figure 2. Fracture test results of SFRC-OL, SFRC3D and SFRC-5D

In Figure 2 it can be seen that when the fibre type changes the fracture behaviour of the SFRC studied dramatically varied. It can be seen that the overall best performance was obtained with the 3D fibres, followed by the 5D fibres and lastly by the OL fibres. SFRC-3D reached the highest load (maximum load and remaining load) followed by SFRC-5D and SFRC-OL. It should be also mentioned that in SFRC-5D and SFRC-3D alike the maximum load appeared around 1 mm of CMOD while in SFRC-OL the maximum load was reached at a CMOD around 0.125 mm. After reaching the maximum load, all concrete specimens showed a progressive unloading.

Preprints (www.preprints.org) | NOT PEER-REVIEWED | Posted: 30 November 2021 doi:10.20944/preprints202111.0566.v1

The fracture behaviour of the concrete mixes where cocktail of fibres was added can be seen in Figure 3.

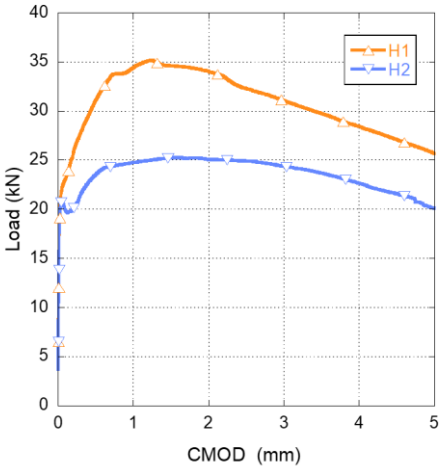

Figure 3. Fracture test results of H1 and H2.

In Figure 2 and Figure 3 the curves shown correspond to at least the average behaviour of three specimens. It should be also highlighted that no remarkable scattering was found in the tests. Regarding the fracture behaviour of the mentioned formulations, it can be stated that the cocktails used in H1 and H2 clearly enhanced the fracture behaviour of any of the formulations that had only one type of fibres.

In order to determine if it is possible to consider the contribution of the fibres in the structural design, and consequently to reduce the amount of steel reinforcement, [20] sets that the strength of the material at a CMOD value of 0.5 mm, which is often known as f_{R1} should be at least 40% of the load at the limit of proportionality (f_{LOP}). Moreover, it should be also checked that the load at a CMOD value of 2.5 mm should be at least 20% of f_{LOP}, being usually termed f_{R3}. In Table 4 it can be observed that all concrete formulations exceed the requirements set by [20].

Table 4. Residual strength of the concrete formulation in relation with the requirements set by [20].

Strength (MPa)	f_{LOP}	f_{R1} (0.5mm)	% f_{LOP}	f_{R3} (2.5mm)	% f_{LOP}
SFRC-OL	7.3	7.39	102%	5.03	69%
SFRC-5D	5.5	8.11	148%	8.40	153%
SFRC-3D	8.2	13.18	161%	12.17	148%
H1	7.0	9.94	142%	10.33	147%
H2	6.6	7.51	113%	7.97	120%

Similarly to what was mentioned in the case of the production process, a detailed description and discussion of the results can be found in [23]

3 Numerical simulations

The concept of the cohesive crack zone [28-30] is implemented in an element formulation, with and embedded cohesive crack, in order to reproduce the cracking process of the concrete formulations. Although this concept was firstly developed for plain concrete [31] it has been subsequently applied in fibre cementitious materials with successful results [32]

This approach considers that fracture takes place in mode I and hence it is assumed that the cohesive stress vector **t** transmitted across the crack faces is parallel to the crack displacement vector **w** (central forces model). If the magnitude of the crack opening vector $|\mathbf{w}|$ does not decrease the relation between both parameters can be stated as appear in (1)

Preprints (www.preprints.org) | NOT PEER-REVIEWED | Posted: 30 November 2021 doi:10.20944/preprints202111.0566.v1

$$\mathbf{t} = \frac{f(|\mathbf{w}|)}{|\mathbf{w}|}\mathbf{w} \quad (1)$$

Where $f(|\mathbf{w}|)$ is the softening function for pure opening, that in this manuscript will be defined by multilinear functions which unloading and reloading branches are aligned with the origin and the softening function is defined by a set of points.

The mentioned formulation is referred to constant strain triangular elements that only have one integration point. It should be mentioned that only the directions parallel to the triangle sides are considered as cracking directions. If the element cracks such discontinuity appears crossing the barycentre of the triangle.

If the element is cracked, and consequently the crack direction is determined, the stress vector $\mathbf{t}$ can be obtained as

$$\mathbf{t} = \frac{A}{hL}\boldsymbol{\sigma}\,\mathbf{n} \quad (2)$$

It should be mentioned that the stress vector $\mathbf{t}$ is constant along the crack, being h the triangle height, A represents the area of the element, L the crack length, $\boldsymbol{\sigma}$ the stress tensor and $\mathbf{n}$ the unit vector normal to that side and to the crack. A more detailed explanation of the implementation can be found in [32].

In the cohesive crack theory, it is assumed that outside the crack the material remains elastic. The stress tensor can be obtained using (3) where the inelastic behaviour is subtracted to correct the elastic deformation of the element by including the crack displacement.

$$\boldsymbol{\sigma} = \mathbf{E}\colon[\varepsilon^{\alpha} - (\mathbf{b}^{+}\otimes\mathbf{w})^{S}] \quad (3)$$

In (3) $\mathbf{E}$ stands for the elastic tangent tensor $\varepsilon^{\alpha}$is the apparent strain vector obtained with the nodal displacements and $\mathbf{b}^{+}$is the gradient vector corresponding to the shape function of the solitary node as appears in (4)

$$\mathbf{b}^{+} = \frac{1}{h}\mathbf{n} \quad (4)$$

If it is considered that $\mathbf{t} = \boldsymbol{\sigma}\,\mathbf{n}$ and also using (1) and (3) the following expression could be obtained.

$$\left[\frac{f(|\tilde{\mathbf{w}}|)}{|\tilde{\mathbf{w}}|}\mathbf{1} + [\mathbf{n}\cdot\mathbf{E}\colon\mathbf{b}^{+}]\right]\mathbf{w} = [\mathbf{E}\colon\varepsilon^{\alpha}]\cdot\mathbf{n} \quad (5)$$

Where $\mathbf{1}$ stands for the identity tensor. If an iterative algorithm is used $\mathbf{w}$ could be found to satisfy (5).

The approach previously explained was introduced in a material subroutine in a finite element code seeking to reproduce the material behaviour. An external file with the coordinates of the nodes and the elements is required to feed the subroutine with the geometry of the elements. If the material has not reached the tensile strength (f_{ct}) the element behaves elastically. On the contrary, if such value is exceeded, the direction of the maximum principal stress is found and a crack perpendicular to such direction is introduced. From that point onwards the behaviour of the element is governed, if strains keep growing, by the softening function of the material which relates the stress and the crack opening relation (σ-w). Apart from the tensile strength the subroutine requires the modulus of elasticity of the material E.

The shape and characteristic points of the softening functions were determined based on an iterative inverse analysis. Such process can be summarised as the following steps. Firstly, the softening function is implemented in the element and the points that define it are set. Secondly, the simulation is performed and the behaviour of the numerical model when subjected to the fracture test obtained. Thirdly, the experimental and the numerical behaviours are compared. This can be carried out using the load-deflection of the load-crack mouth opening displacement (CMOD) curves. If the numerical behaviour does not reproduce the experimental behaviour, the points that define the softening function are modified and the next iteration starts again. If the numerical behaviour simulates with a certain degree of accuracy the experimental behaviour the points proposed in the first step are considered valid.

Preprints (www.preprints.org) | NOT PEER-REVIEWED | Posted: 30 November 2021 doi:10.20944/preprints202111.0566.v1

In order to reproduce the material behaviour a plane mesh with plane stress conditions has been employed. The mesh is composed by constant strain triangles which are finer in the whereabouts of the notch. An image of one of the meshes can be seen in Figure 4. This scheme of mesh has been considered valid in [33, 34].

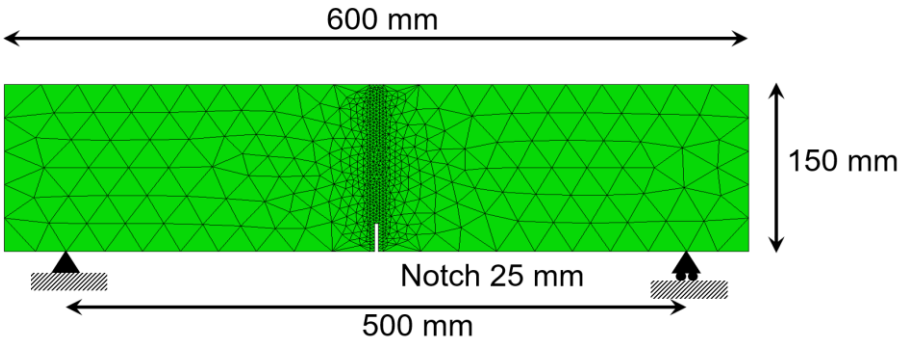

Figure 4. Mesh used in the numerical simulations.

4. Results and discussion

In figure 5(a) the comparison of the results obtained in the experimental campaign and the simulations are compared. As it can be clearly observed the degree of accuracy that has been achieved is remarkable being the only slight difference present in the peak load. In contrast to what was shown in [32] the softening function in this occasion was composed by four straight stretches. The first one starts when the opening of the crack is null and the stress is equal to the tensile strength registered in tests carried out in plain concrete. There is a sudden drop of the load bearing capacity of the material in the initial stretch that might be related to the crack width required by the fibres to contribute to the strength of SFRC-OL. Once the fibres start to enhance the mechanical properties of the concrete matrix the load bearing capacity decrease is more gradual. Such feature is also perceived in the last to stretches of the softening function.

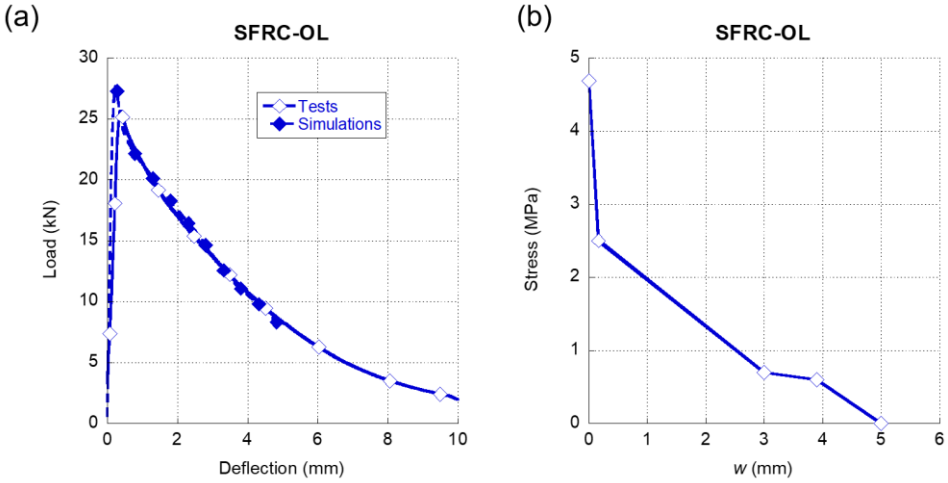

Figure 5. (a) Comparison of the average experimental results obtained in the fracture tests of SFRC-OL and the numerical simulation. (b) softening function used in the simulation shown in (a).

Similarly to Figure 5, in Figure 6 (a) it can be seen the comparison between the experimental results registered when testing SFRC-3D in a three-point bending fracture test and the results that were obtained in the numerical simulations. It should be highlighted that the accuracy of the simulation is remarkable not only in the peak load but also throughout the unloading branch of the test. Moreover, even at deflection values beyond 6 mm the simulation was able to replicate the behaviour of SFRC-3D with precision. Regarding the softening function that enable such accuracy, which is shown in Figure 6(b) it should be

Preprints (www.preprints.org) | NOT PEER-REVIEWED | Posted: 30 November 2021 doi:10.20944/preprints202111.0566.v1

underlined that, in contrast to what was shown in Figure 5(b) there is no initial steep unloading for reduced crack widths. On the contrary, it can be perceived in Figure 6(b) that the initial part of the softening function maintains the load bearing capacity close to the tensile strength of plain concrete. Such feature might be related with the shape of the fibres that boasted hooked ends. Once this initial stretch is surpassed, there is a progressive loss in the load bearing capacity of SFRC-3D which is notoriously steeper than the first stretch.

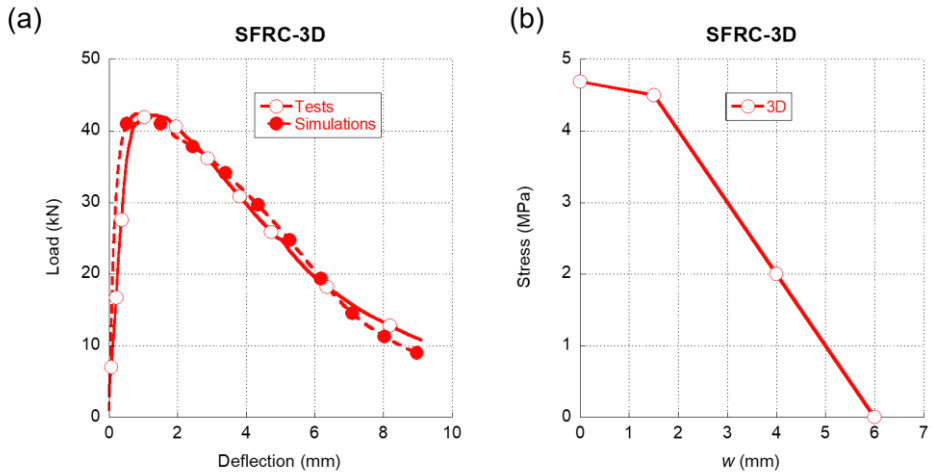

Figure 6. (a) Comparison of the average experimental results obtained in the fracture tests of SFRC-3D and the numerical simulation. (b) softening function used in the simulation shown in (a).

In Figure 7(a) it can be observed the comparison between the experimental results of the three-point bending fracture tests of SFRC-5D and their numerical reproduction. The dashed line that represents the numerical simulation clearly follows the experimental trends with accuracy. The peak load is captured with precision and even the progressive loss of stiffness that the material suffers before reaching such point is reproduced. Moreover, there is an almost identical unloading in the simulation and in the experimental test from the peak to the end of the test. Concerning the softening function that enables such accurate simulation, it should be mentioned that in contrast with what was shown in Figure 6(b) the softening function of SFRC-5D that can be seen in Figure 7(b) boasts a sudden decrease of the load bearing capacity after surpassing the tensile strength. This phenomenon was not expected because such load drop did not appear in the case of 3D fibres. If the crack width continues to grow the load bearing capacity increases up to a local maximum which is followed by the final unloading of the material.

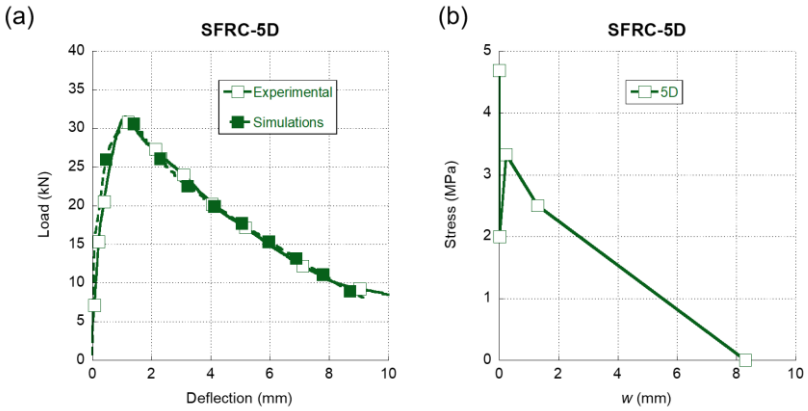

Figure 7. (a) Comparison of the average experimental results obtained in the fracture tests of SFRC-5D and the numerical simulation. (b) softening function used in the simulation shown in (a).

In this manuscript not only the experimental curves of the three-point bending fracture tests of the formulations with the addition of one fibre have been simulated but also the formulations with an addition of cocktail of fibres. In the case of the formulation H1 the cocktail of fibres was composed by OL fibres and 5D fibres. At this point it should be

Preprints (www.preprints.org) | NOT PEER-REVIEWED | Posted: 30 November 2021 doi:10.20944/preprints202111.0566.v1

mentioned that the fracture curve was simulated following the same iterative process that was applied to the concrete formulation with only one type of fibre. Consequently, although the softening functions of SFRC-OL and SFRC-5D were known the softening function of H1 could not be inferred from them.

In Figure 8(a) it can be seen the comparison between the three-point bending fracture tests of H1 and the results obtained in the simulations. It can be observed that the simulations with the softening function shown in Figure 8(b) posse a high resemblance with the experimental results both in the loading and unloading part of the curve. Regarding the softening function, it should be underlined that it features the initial sudden load bearing capacity drop typical of 5D fibres. Besides, the same steep recovery appears right after the initial unloading has taken place. After reaching the maximum of this second stretch there is a progressive unloading until the total collapse of the material. It should be also mentioned that the maximum crack width in the softening function of H1 is greater than any of the concrete formulations that had only one type of fibre.

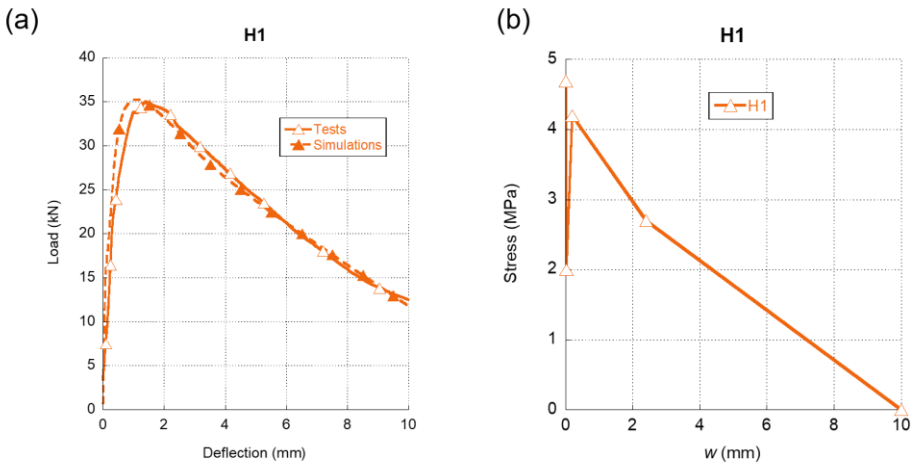

Figure 8. (a) Comparison of the average experimental results obtained in the fracture tests of H1 and the numerical simulation. (b) softening function used in the simulation shown in (a).

Regarding the fracture behaviour of H2, in Figure 9(a) it can be observed the precision obtained in the simulations if such results are compared with the experimental ones. It should be emphasised that the numerical simulations were able of reproducing not only the initial loading stretch but also the progressive loss of stiffness that the material suffers after reaching 20 kN until the peak load of the test is registered. It should be also mentioned that, as it happened in the SFRC-5D and SFRC3D tests, the peak load is registered gradually in contrast to the abrupt loss of stiffness observed in SFRC-OL. Such feature entails that the presence of 5D fibres are capable of sustaining loads for reduced deflections. These two characteristics of the experimental curve are notably well captured by the numerical simulations. Moreover, a great similarity of the experimental and the numerical curves can be seen between during the complete test. If Figure 9(b) is analysed, it can be mentioned that there is a sharp decrease of the load bearing capacity of the material right after surpassing the tensile strength of plain concrete. Nevertheless, it can be also said that the presence of 5D and PF fibres enable H2 to partially recover the load bearing capacity even at low values of crack openings. Considering the notorious differences between the modulus of elasticity of 5D and PF fibres, 5D fibres might be considered the main responsible for such recovery. Another characteristic that should be underlined is that the maximum crack opening for this cocktail of fibres is remarkably greater than the ones shown in SFRC-3D, SFRC-5D and SFRC-OL formulations.

Preprints (www.preprints.org) | NOT PEER-REVIEWED | Posted: 30 November 2021 doi:10.20944/preprints202111.0566.v1

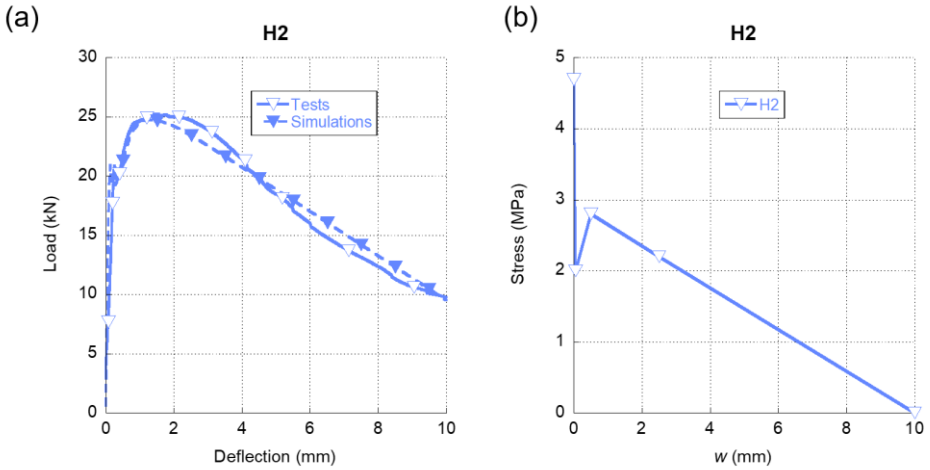

Figure 9. (a) Comparison of the average experimental results obtained in the fracture tests of H1 and the numerical simulation. (b) softening function used in the simulation shown in (a).

The accuracy of the simulations performed in all the concrete mixes can be assessed by comparing the fracture energies that are obtained in the experimental tests and the numerical simulations. In the last column of Table 5 the relative error of the fracture energy simulated can be seen being in all cases below 2%.

Table 5. Comparison of the experimental and simulated fracture energies at a deflection of 10mm.

Concrete mix	Experimental W_f (kN/mm)	Simulation Wf (kN/mm)	Experimental G_f (N/m)	Simulation G_f (N/m)	ΔGf (%)
SFRC-OL	98,8	97,1	5270,4	5179,7	-1,75%
SFRC-3D	236,8	241,5	12627,8	12878,1	1,94%
SFRC-5D	170,5	172,8	9095,8	9213,9	1,28%
H1	232,4	235,2	12396,2	12546,1	1,20%
H2	178,9	181,1	9542,9	9657,4	1,19%

5. Discussion

In Figure 10 (a) comparison of the softening functions of the SFRC formulations with only one type of fibre addition can be observed. It is obvious that there are great differences among the three curves. The first feature that can be noted is that in the case of the SFRC-OL and SFRC-5D formulations right after surpassing the tensile strength a sudden drop of the load bearing capacity of the material appears. While this might be expected in the case of the SFRC-OL formulation due to the straight shape of the OL fibres, in the case of the 5D fibres the double hook present in the ends of the fibres might have prevented any unloading from happening. Moreover, when seeking to determine the softening function of SFRC-5D it became evident that the slight reduction of the stiffness that appears in the load-deflection curves shown in Figure 7 (a) is greatly influenced by this stretch of the softening function. In contrast to what has been previously explained, the first stretch of the SFRC-3D softening function shows that the fibres can bear the load that the concrete matrix transfers to them when the tensile strength of the concrete is reached. thus, such stretch only shows a slight unloading.

After the first stretch, the softening function of the SFRC-OL fibres continues to develop a progressive unloading until the failure of the material takes place. It should be mentioned that the slope of the rest of the unloading stages are much more progressive than the first stretch. This feature confers SFRC-OL a certain ductility. Regarding the remaining part of the SFRC-3D softening function it can be seen in Figure 10(a) that there is

Preprints (www.preprints.org) | NOT PEER-REVIEWED | Posted: 30 November 2021 doi:10.20944/preprints202111.0566.v1

a load drop stretch until the collapse of the material happens. On the contrary, the softening function of SFRC-5D boasts an increment of the load bearing capacity in the second stretch of the curve. Such increment might be a result of a proper anchorage between the fibres and the concrete matrix. Once the anchorage fails, the material begins to unload until the failure is produced. Another feature that should be mentioned is that in all concrete formulations the maximum crack width is greater that the length of the fibres added being no evident relation with the fibre length. Such relation is more evident in the case of OL fibres which fibre length is 13 mm and the maximum crack width is only 5mm. Similarly, the length of 5D fibres is equal to 60 mm while the maximum crack width is 8.3 mm. An analogue comment can be performed regarding 3D fibres.

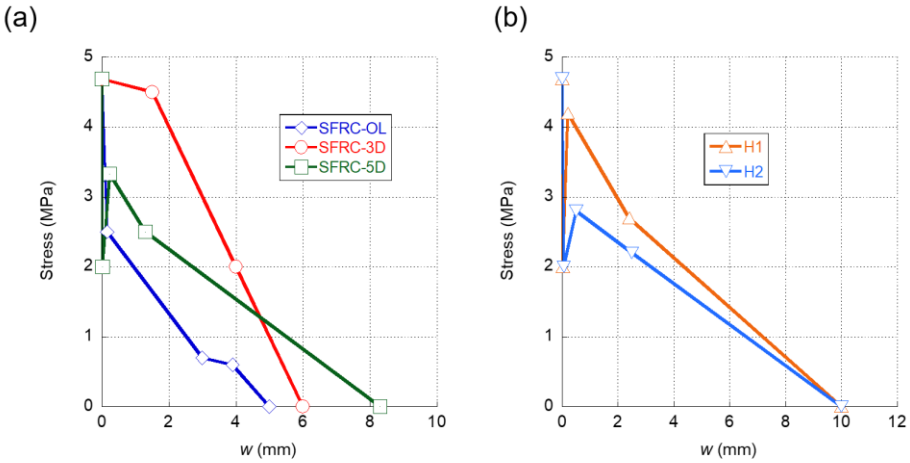

Figure 10. (a) Softening functions obtained in the inverse analysis of SFRC-OL, SFRC-3D and SFRC-5D (b) Softening functions obtained in the inverse analysis of H1 and H2.

In the case of the softening functions of the H1 and H2 formulations, it can be observed in Figure 10 (b) that they boast similar shapes. Both of them have a rapid reduction of the load bearing capacity right after reaching the tensile strength of the concrete matrix. This might be explained by the presence of 5D and OL fibres in both formulations. Moreover, in the case of H2 the presence of PF fibres in the fibre cocktail may have been also related with this feature. Regarding the re-loading stage of both softening functions, the H1 formulation was capable of gaining stress up to values close to the tensile strength of plain concrete. This feature might be caused by the greater proportion of 5D fibres present in the H1 mix. On the contrary H2 boast a re-loading stage more subtle and with less slope than the correspondent stretch of H1. As was stated in [35] the softening functions that can represent the fracture behaviour of PFRC mixes boast a reloading stage after the first unloading. Therefore, such changes might be accounted for the presence of a greater number of 5D fibres in H1 and also to the lower modulus of elasticity of the PF fibres present in H2. Another feature that should be underlined is that the softening functions of H1 and H2 alike have maximum crack width that is greater than any of the softening functions of the fibres individually. This increment of the maximum crack width might be an effect of the synergies that appear when cocktails of fibres are used.

6. Conclusions

This study has implemented multi-linear softening functions in a user material subroutine of a finite element code, by means of an embedded cohesive crack in a finite element, in order to simulate the three-point bending fracture behaviour of three concrete mixes obtained adding to a plain concrete 0.89% volume fraction of OL, 3D and 5D fibres in each. In addition, the fracture behaviour of the same plain concrete with a cocktail of OL and 5D fibres and another cocktail of OL, 5D and PF maintaining the same fibre volume fraction were also reproduced. It should be mentioned that the approach based on the multilinear softening functions has proved to be a robust and efficient method to simulate the fracture behaviour of the concrete mixes analysed.

The mentioned approach has been capable of reproducing the fracture behaviour of the five concrete types studied with accuracy. Not only the shapes of the experimental load-deflection curves were accurately simulated but also it was observed that the differences between the experimental fracture energy of the material and the numerically obtained are below 2% in all formulations.

The analysis of the softening function correspondent to SFRC-5D showed that the presence of the double-hooked end in 5D fibres might did not provide an increment of the fibre-matrix anchorage for reduced crack widths. However, the double-hooked ends of 5D fibres enabled a re-loading stage for greater crack widths. Moreover, 3D fibres were capable of sustaining the loads transferred by the concrete when the first cracks appear and no load drops appeared at initial crack widths of the SFRC-3D softening function. The softening function of SFRC-OL boasts a progressive unloading of the material when increasing the crack width. Lastly, no relationship was observed between the length of the fibres and the maximum crack width of the softening functions found.

Regarding the softening functions of H1 and H2, it was observed that there was a clear resemblance between them. The presence of OL and 5D fibres in both cocktails explain the presence of an unloading stretch right after surpassing the tensile strength of concrete. Besides, both formulations showed a re-loading stage which is related to the content of 5D fibres in the case of H1 and to the presence of 5D and PF fibres in the case of H2. The lower proportion of 5D fibres and the lower modulus of elasticity of PF explain the differences in the slope of the re-loading stretch.

The synergies that appeared when combining several types of fibres generate an increment of the maximum crack width both in H1 and H2. However, a further analysis should be performed for a better measurement of the enhancement that the combination of fibres can provide.

Author Contributions: The following statements should be used "Conceptualization, A.E, M.G.A and J.C.G..; methodology, A.E, M.G.A and J.C.G.; validation, A.E, M.G.A, J.C.G. and P.C..; formal analysis A.E, M.G.A, J.C.G. and P.C..; investigation, A.E, M.G.A, J.C.G. and P.C.; resources, J.C.G.; data curation, A.E and P.C.; writing—original draft preparation, A.E, M.G.A, J.C.G. and P.C..; writing—review and editing, A.E, M.G.A, J.C.G. and P.C.. funding acquisition, J.C.G. All authors have read and agreed to the published version of the manuscript."

Funding: This research received no external funding.

Acknowledgments: The authors gratefully acknowledge the Ministry of Economy, Industry and Competitiveness of Spain by means of the Research Fund Project BIA2016-78742-C2-2-R. They also offer their gratitude to SIKA SAU and Calle 30 for supporting the Enterprises University Chairs "Cátedra Sika-UPM" and "Cátedra Universidad Empresa Calle30-UPM" respectively.

Conflicts of Interest: The authors declare no conflict of interest.

References

1. Brandt, A. Fibre reinforced cement-based (FRC) composites after over 40 years of development in building and civil engineering. *Compos. Struct.*, **2008**, 86 (1-3), 3-9.
2. Naaman, E. Engineered steel fibers with optimal properties for reinforcement of cement composites. J. *Adv. Concr. Technol*., **2003**, 1(3), 241-252.
3. Zollo, R. Fiber-reinforced concrete: an overview after 30 years of development, *Cem Concr Compos*. **1996**, 19,. 107-122.
4. Pająk, M.; Ponikiewski, T. Flexural behavior of self-compacting concrete reinforced with different types of steel fibers. *Constr Build Mater.* **2013**, 47, 397-408.
5. Giaccio, G.; Tobes, J. M.; Zerbino, R. Use of small beams to obtain design parameters of fibre reinforced concrete. *Cem Concr Compos*, **2008**, 30(4), 297-306.
6. Enfedaque, A.; Alberti, M. G.; Gálvez, J. C. Influence of fiber distribution and orientation in the fracture behavior of polyolefin fiber-reinforced concrete. *Materials*, **2019,** 12(2), 220.
7. Lopez, J. A.; Serna, P.; Camacho, E.; Coll, H.; Navarro-Gregori, J. First ultra-high-performance fibre-reinforced concrete footbridge in Spain: Design and construction. *Struct. Eng. Int.*, **2014** 24(1), 101-104.
8. Jafarifar, N.; Pilakoutas, K.; Bennett, T. The effect of shrinkage cracks on the load bearing capacity of steel-fibre-reinforced roller-compacted-concrete pavements. *Mater. Struct.*, **2016,** 49(6), 2329-2347.

9. De la Fuente, A.; Pujadas, P.; Blanco, A.; Aguado, A. Experiences in Barcelona with the use of fibres in segmental linings. *Tunn. Undergr. Space Technol.*, **2012,** 27(1), 60-71
10. Alberti, M. G., Enfedaque, A., Gálvez, J. C., Pinillos, L. Structural Cast-in-Place Application of Polyolefin Fiber–Reinforced Concrete in a Water Pipeline Supporting Elements. *J. Pipeline Syst. Eng*, **2017**, 8(4), 05017002.
11. Alberti, M.G.; Enfedaque, A.; Gálvez, J.C. Improving the Reinforcement of Polyolefin Fiber Reinforced Concrete for Infrastructure Applications. *Fibers* **2015**, *3*, 504-522. https://doi.org/10.3390/fib3040504.
12. Hossain, K. M. A.; Lachemi, M.; Sammour, M.; Sonebi, M. Strength and fracture energy characteristics of self-consolidating concrete incorporating polyvinyl alcohol, steel and hybrid fibres. *Constr Build Mater*, **2013,** 45, 20-29.
13. Okeh, C. A.; Begg, D. W.; Barnett, S. J.; Nanos, N. Behaviour of hybrid steel fibre reinforced self-compacting concrete using innovative hooked-end steel fibres under tensile stress. *Constr Build Mater*, **2019,** 202, 753-761.
14. Caggiano, A.; Cremona, M.; Faella, C.; Lima, C.; Martinelli, E. Fracture behavior of concrete beams reinforced with mixed long/short steel fibers. *Constr Build Mater*, **2012,** 37, 832-840.
15. Rambo, D. A. S.; de Andrade Silva, F.; Toledo Filho, R. D. Effect of steel fiber hybridization on the fracture behavior of self-consolidating concretes. *Cem Concr Compos*, **2014,** 54, 100-109.
16. Caetano, H.; Rodrigues, J. P. C.; Pimienta, P. Flexural strength at high temperatures of a high strength steel and polypropylene fibre concrete. *Constr Build Mater*, **2019,** 227, 116721.
17. Sivakumar, A.; Santhanam, M. A quantitative study on the plastic shrinkage cracking in high strength hybrid fibre reinforced concrete. *Cem Concr Compos*, **2007,** 29(7), 575-581
18. EHE-08, Spanish Structural Concrete Code, Spanish Minister of Public Works, 2008
19. CNR-DT 204, Guide for the design and construction of fiber-reinforced concrete structures, Consiglio Nazionale delle Riserche, Roma, 2006.
20. MC2010, fib Model Code, Paris: Fédération Internationale du Béton fib/International Federation for Structural Concrete, 2010.
21. Sucharda, O.; Pajak, M.; Ponikiewski, T.; Konecny, P. Identification of mechanical and fracture properties of self-compacting concrete beams with different types of steel fibres using inverse analysis. *Constr Build Mater*, **2017,** 138, 263-275.
22. Gao, D.; Ding, C.; Pang, Y.; Chen, G. An inverse analysis method for multi-linear tensile stress-crack opening relationship of 3D/4D/5D steel fiber reinforced concrete. *Constr Build Mater*. **2021**, 309, 125074.
23. Alberti, M. G.; Enfedaque, A.; Gálvez, J. C.; Cortez, A. Optimisation of fibre reinforcement with a combination strategy and through the use of self-compacting concrete. *Constr Build Mater*, **2020,** 235, 117289.
24. EN 12390-3, Testing hardened concrete. Part 3: Compressive strength of test specimens, **2009**
25. EN 12390-13, Testing hardened concrete – Part 13: Determination of secant modulus of elasticity in compression, **2013**
26. EN 12390-6, Testing hardened concrete. Part 6. Tensile splitting strength of test specimens, **2009**
27. EN 14651:2005+A1, Test method for metallic fibre concrete. Measuring the flexural tensile strength (limit of proportionality (LOP), residual), **2007**
28. Hillerborg, A.; Modéer, M.; Petersson, P. E. Analysis of crack formation and crack growth in concrete by means of fracture mechanics and finite elements, *Cem Concr Res,* **1976,** 6(6), 773-78, 1976
29. Barenblatt, G. I. The mathematical theory of equilibrium cracks in brittle fracture. In Advances in applied mechanics, **1962**, 7, 55–129. Elsevier,
30. Dugdale, D. S. Yielding of steel sheets containing slits. J *Mech Phys Solids*, **1960,** 8(2), 100–104
31. Guinea, G. V.; Planas , J.; Elices, M. A general bilinear fit for the softening curve of concrete. *Mater. Struct.,* **1994**,. 27,. 2,. 99-105.
32. Enfedaque, A.; Alberti, M.G.; Gálvez. J.; Domingo, J. Numerical simulation of the fracture behaviour of glass fibre reinforced cement, *Constr Build Mater,* **2017,** 136, 108-117.
33. Suárez, F.; Gálvez, J. C.; Enfedaque, A.; Alberti, M. G. Modelling fracture on polyolefin fibre reinforced concrete specimens subjected to mixed-mode loading, *Eng Fract Mech*. **2019,** 211, 244-253.
34. Suárez, F., Gálvez, J. C.; Alberti, M. G.; Enfedaque A. Fracture and size effect of PFRC specimens simulated by using a trilinear softening diagram: A predictive approach. *Materials* **2021,** 14(14).
35. Alberti, M. G.; Enfedaque, A.; Gálvez, J. C.; Reyes, E. Numerical modelling of the fracture of polyolefin fibre reinforced concrete by using a cohesive fracture approach. *Compos. B. Eng*., **2017** 111, 200-210.